Juan S. Acero Triana[1], Hoori Ajami[1]

[1]Department of Environmental Sciences, University of California, 2460A Geology Building,

Riverside, CA 92521, USA.

Corresponding author: Juan S. Acero Triana (juanseba@ucr.edu)

Key Points:

- Quantifying relative contribution of climate and anthropogenic stressors in water budget of managed endorheic basins is challenging.
- Time series decomposition approaches identify key water balance variables responsible for endorheic lake depletion.
- Clustering of decomposed time series reveal structural behavior of water balance components, and trace sources of system alterations.
- Decreases in the Colorado River allocation are causing the Salton Sea to shrink, not changes in the irrigation operation or local climate as commonly believed.

Abstract

The fragile balance of endorheic lakes in highly managed semi-arid basins with transboundary water issues has been altered by the intertwined effects of global warming and long-term water mismanagement to support agricultural and industrial demand. The alarming rate of global endorheic lakes' depletion in recent decades necessitates formulating mitigation strategies for ecosystem restoration. However, detecting and quantifying the relative contribution of causal factors (climate variability and anthropogenic stressors) is challenging. This study developed a diagnostic multivariate framework to identify major hydrologic drivers of lake depletion in a highly managed endorheic basin with a complex water distribution system. The framework integrates the Soil and Water Assessment Tool (SWAT) simulations with time-series decomposition and clustering methods to identify the major drivers of change. This diagnostic framework was applied to the Salton Sea Transboundary Basin (SSTB), the host of the world's most impaired inland lake. The results showed signs of depletion across the SSTB since late 1998 with no significant changes in climate conditions. The time-series data mining of the SSTB water balance components indicated that decreases in lake tributary inflows (-16.4 Mm3 yr-2) in response to decline in Colorado River inflows, associated with state water transfer agreements, are causing the Salton Sea to shrink, not changes in the irrigation operation as commonly believed. The developed multivariate detection and attribution framework is useful for identifying major drivers of change in coupled natural-human systems.

1 Introduction

Endorheic basins and lakes play a crucial role in hydro-ecological functioning and aquatic biodiversity of arid and semi-arid regions (Donnelly et al., 2020;

Sheng, 2020). These ecosystems represent approximately 25% of Earth's land surface area and 50% of the world's water-stressed regions (J. Wang et al., 2018a; Yapiyev et al., 2017), provide numerous ecosystem services to humans (e.g., water and food supply, pollutant retention, and recreation), and serve as critical habitats for aquatic, semi-aquatic, and riparian wildlife and unique microorganisms (Oren, 2013; Zadereev et al., 2020). Despite the importance of endorheic basins for local and regional ecological functioning, they are one of the most threatened ecosystems in the world, with an increasing number of threatened and endangered species (Saccò et al., 2021; Zadereev et al., 2020). The endorheic lakes have shrunk globally at an alarming rate in recent decades due to the combined effects of global warming and long-term water mismanagement to support agricultural and industrial demand, altering the fragile balance of these ecosystems. Recent hydrologic studies have shown that between 2002 and 2016, the global endorheic system has lost on average 106.3 Gt yr^{-1} of water storage, representing twice the loss observed in exorheic counterpart (J. Wang et al., 2018b). While (freshwater) exorheic ecosystems have long been recognized as important resource, programs to protect (saline) endorheic lakes have been relegated significantly (Williams, 2002). Therefore, formulating mitigation strategies to restore and protect endorheic basins and lakes is urgent and imperative.

Prior to formulating these strategies, it is crucial to understand and simulate the hydrologic response mechanisms of endorheic ecosystems to natural and anthropogenic stressors, and identify the causal factors that have caused their environmental deterioration (Saccò et al., 2021). However, quantifying the relative contribution of climate variability and anthropogenic stressors in water budget dynamics of endorheic basins and lakes is challenging (Li et al., 2018). Hydrologic processes of highly managed agroecosystems are complex, and the lack of high-resolution spatial and temporal water budget data in endorheic basins with transboundary water issues further contributes to this problem. Water resources management under global warming hinders the efforts to solve water conflicts in endorheic basins as stakeholders tend to be reluctant to share information that may alter previously gained water rights (Yapiyev et al., 2017). These circumstances limit the scope of modeling studies, which aim to holistically consider coupled natural-human system dynamics and identify major hydrologic change drivers of lake dynamics at the basin scale. Although some studies have used mass balance approaches (e.g., stock-flow and statistical models, satellite altimetry) to understand lake budgets and storage changes (Mohammed & Tarboton, 2012; Schulz et al., 2020; J. Wang et al., 2018a; Yao et al., 2018; Yapiyev et al., 2019), very few attempted to understand basin processes and the lake-basin interactions (Dehghanipour et al., 2020; Tian et al., 2015; Zhou et al., 2015). Dehghanipour et al. (2020) and Tian et al. (2015) developed a scenario-based approach using WEAP-MODFLOW (coupled planning-groundwater model) and GSFLOW (coupled surface water-groundwater model), to understand variable interrelationships and water conflicts in two endorheic irrigated basins in Iran and China, respectively. Zhou et al. (2015) employed WEB-DHM (coupled

biosphere-hillslope hydrological model) to evaluate the relationship between lake water storage changes and the variability of precipitation, lake inflows, and evapotranspiration in a rainfed central Tibetan Plateau basin in China.

This study aims to develop a hydrologic modeling framework to simulate long-term patterns of lake-basin interactions and identify major hydrologic change drivers in highly managed endorheic basins with complex water distribution systems. Our virtual hydrologic laboratory is the Salton Sea Transboundary Basin (SSTB) in the US-Mexico border between California and Baja California Norte, and the host of the most impaired inland lake in the world. The Salton Sea volume has declined by 32% over the last 25 years leading to its eutrophication and hyper-salinization and exposure of its toxic playa. These conditions have threatened aquatic life including threatened and endangered species in the region and have caused major public health issues due to low air quality (Frie et al., 2019; Jones & Fleck, 2020). The causes of Salton Sea environmental crisis and lake level decline are not fully understood, and several possible factors are acknowledged such as the dispute for the Colorado River allocations among seven US states and between the US and Mexico, decrease in the irrigation return flow due to irrigation efficiency, changes in the lake-groundwater interactions, global warming, and the combined effect of several or all the above factors.

Given the complexity of ecohydrological processes that control lake level fluctuations, this study addresses the following fundamental research questions: (1) how the water balance partitioning of a highly managed endorheic basin with complex water distribution system has changed over the past four decades? (2) what are the spatio-temporal relationships among the potential hydrologic drivers of the SSTB water balance changes and their influence on the trend and seasonality of the water balance components? and (3) what are the relative contribution of climate and land and water management practices as the major hydrologic drivers of an endorheic lake water level depletion? To address these questions, we integrated the semi-distributed Soil and Water Assessment Tool (SWAT) with time series data mining techniques to quantify regional water balance and understand interrelationships among hydrological and management variables in an endorheic basin, SSTB, that relies on imported Colorado River inflow for agricultural productivity. This study introduces a robust multivariate methodology for detection and attribution of major hydrologic change drivers of lake storage changes, enabling evaluation of potential environmental trade-offs to formulate SSTB restoration strategies. Our multivariate detection and attribution approach can be used in managed endorheic basins elsewhere.

2 Materials and Methods

2.1 Study area

The SSTB encompasses 21,600 km^2 and is located at the fringe of warm arid (Kottek et al., 2006) North American Deserts Ecoregion in the US-Mexico border between California and Baja California Norte (Figure 1e-f). Long-term annual mean precipitation is 178 mm, and it follows a bimodal distribution with maxi-

mum in February and December. Long-term mean temperature is 20.7 °C and may vary between -5.1 and 46.5 °C, with the maximum and minimum usually observed in July-August and December-January, respectively. The SSTB is an enclosed inland system (endorheic basin) with mountains in the north and west, and a valley in the center. Elevations range from -72 to 3,502 m above mean sea level (Figure 1a). The soils are primarily unweathered bedrocks and gravels in the higher elevations and silty clay loams and loamy fine sands in the valleys (Figure 1d) (NRCS, 2016). Soils are mainly composed of 1–2 horizons extending to a maximum depth of 1.5 m. Major land cover in the basin is shrubland (49%) and barren land (20%), and the remaining portion consists of cropland (14%), open water (5%), and grassland (4%) (Figure 1f) (CONABIO, 2017; SIGA-BC, 2016; USDA-NASS, 2009). Although the percentage of agriculture is relatively small, the Mexicali, Imperial, and Coachella Valleys (MV, IV, CV) represent some of the most productive agricultural regions in North America, with field crops (e.g., alfalfa, wheat) being the predominant commodities (Figure 1f).

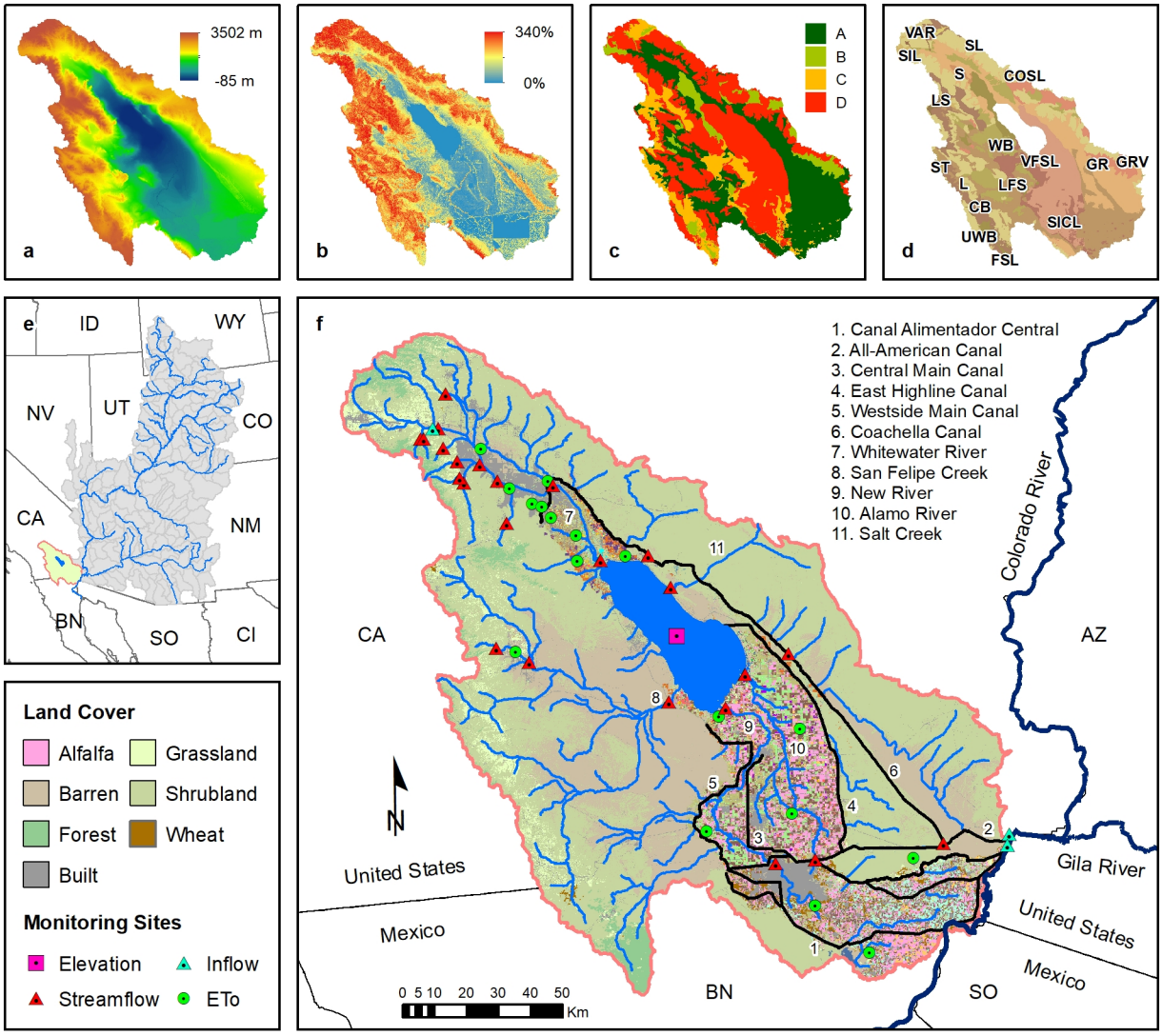

Figure 1. Main features of the Salton Sea Transboundary Basin (SSTB). (a) 30-m digital elevation model (USGS, 2019); (b) 30-m slope; (c) soil hydrologic groups (NRCS, 2016); (d) soil textures (NRCS, 2016); (e) location of the Colorado River Basin (CRB) and SSTB; (f) land cover (CONABIO, 2017; SIGA-BC, 2016; USDA-NASS, 2009), hydrography and main canal system, as well as monitoring networks.

Given the water-stressed condition of the SSTB, the agricultural production is mainly sustained by the imported Colorado River inflows (~152 m^3 s^{-1}). The Colorado River water is diverted at the Imperial and Morelos Dams for transfer

to American and Mexican territories via the All-American and Coachella Canals, and the Canal Alimentador Central, respectively (Figure 1e-f). Smaller lateral canals/pipelines throughout the three valleys distribute the water from main canals to individual fields (CVWD, 2021; IID, 2021). Surface and subsurface losses from irrigation ultimately reach the Salton Sea (SS) via four major tributaries, the Alamo (~23 m^3 s^{-1}) and New (~17 m^3 s^{-1}) Rivers and East Highline Canal (no records) in the south, and Whitewater River (~2 m^3 s^{-1}) in the north. Both Alamo and New Rivers originate in Mexico (Figure 1f); however, the New River flows at the international border (~5.1 m^3 s^{-1}) are the major source of delivery to the American territory. Since 1995, almost all the Alamo River's flow in Mexico has been diverted into the New River through the Mexicali Valley agricultural drainage system and via a weir constructed by the Mexican Water Commission right near the border (Bernal et al., 1999). The Salt and San Felipe Creeks, in the east and west side of Salton Sea, respectively, contribute small inflows (~0.2 m^3 s^{-1}) to the sea.

The Salton Sea is the largest inland lake in California with a mean surface area of approximately 890 km^2 over the last decade. The lake was formed by unexpected flooding events in the Colorado River in the early 1900s (Meyer & van Schilfgaarde, 1984). Expansion of irrigated agriculture in the 1920s across the Imperial and Mexicali Valleys and increased agricultural return flows increased the lake volume by 141% (average 0.25 Mm^3 yr^{-1}) until 1995, with the maximum stored volume of ~9.4 km^3. For several decades, the Salton Sea provided diverse recreational activities (e.g., tourism, fishing, boating) and a critical habitat for approximately 400 bird species along the Pacific Flyway (Audubon California, 2021; Hely et al., 1966; State of California Salton Sea Management Program, 2021). Over the last 25 years, the Salton Sea volume has declined by 3.1 km^3 (-32%), causing the hyper-salinization and eutrophication of the lake, massive bird and fish die-off, and regional asthma crisis due to the spreading of toxic dust from the exposed playa.

2.2 Hydrologic model set-up

A semi-distributed watershed model using SWAT was developed to understand the hydrologic response mechanisms of the Salton Sea and simulate water balance of a highly managed agroecosystem with complex water distribution systems. In SWAT, the spatial heterogeneity of each subbasin is represented by independent hydrologic response units (HRUs) characterized by similar land cover, soil type, and slope. Hydrologic fluxes such as rainfall-runoff, snowmelt, and evapotranspiration are computed at an HRU scale, and the subbasins that each drain a single stream, route the flow following the topographic gradients. SWAT enables representing anthropogenic features such as water imports, transfers, and reservoirs in a simulation framework.

The minimal input data to SWAT includes elevation, soil physical and chemical properties, land cover and management practices, and climate records. As delineation and spatial discretization of an endorheic basin are challenging, we used a 30-m DEM (USGS, 2019), the main water bodies and canals' hydrography

dataset (USGS, 2020), and the ArcHydro Tools with a minimum drainage area of 3 km^2 to delineate streams and subbasins. The streams were then manually adjusted to ensure correct streams connectivity and flow direction resulting in 268 subbasins/streams. Some of these streams were created inside the actual lake area, and a reservoir was assigned as a point sink along the highest order stream to mimic the lake and endorheic configuration of the basin.

Given the hilly terrain in the northern and western parts of the basin, slopes ranged from 0 to 340% (Figure 1b). Slopes were grouped into two main classes, and the mean slope (i.e., 26.7%) was used as a threshold to reduce the number of HRUs and computational cost. The US portion of the SSTB has thirty-nine different soil types based on the State Soil Geographic Database (STATSGO2) (NRCS, 2016). As a similar soil database is not available for the Mexican portion, a random forest classifier was developed in R (R Core Team, 2019; Wright & Ziegler, 2017) to predict the missing data in Mexico. The classifier predicts the STATSGO2 map unit key (mukey) codes using 250-m resolution raster maps of predictors such as latitudes and longitudes, elevation, general land cover, soil bulk density and clay, sand, silt, and coarse fragments content for six soil layers in the entire study area (ISRIC, 2020; Poggio et al., 2021). The classifier with 450 trees and sampling the 34 predictor variables at each split was the most satisfactory model with error values less than 5% for both training and validation. The final soil layer (Figure 1d) extends to a maximum depth of 1.5 m and predominantly consists of silty clay loam, loamy fine sand, and fine sandy loam in the valleys and unweathered bedrock, gravel, and very cobbly in the rest of the basin. Soils in the Mexicali and Coachella Valleys have a high and moderately high drainability (i.e., soil hydrologic groups A and B), respectively, while Imperial Valley soils have low drainability (i.e., group D) (Figure 1c).

The 2008 NASS (USDA-NASS, 2009), 2010 CONABIO (CONABIO, 2017), and 2016 SEDAGRO (SIGA-BC, 2016) cropland data layers were combined and parametrized based on the SWAT plant growth database (Arnold et al., 2012) to create a consistent dataset (Figure 1f) with 29 unique land covers including 15 under agricultural production. Irrigation and subsurface tile drains were implemented in SWAT for these 15 land covers across the Coachella and Imperial Valleys. Tile drains were set at 1-m depth and 15-m spacing with a drainage coefficient of 10 mm d^{-1} (Koluvek, 1964; Montazar, 2021; Pillsbury, 1957). The effective radius of drains and the lateral to vertical saturated conductivity ratio were initially set to 20 mm and 1, respectively, and then adjusted at the subbasin scale during calibration. Automated crop irrigation was applied using the heat-unit approach and an initial water stress of 0.9 to incorporate climate variability impacts on field operation dates. The main canal system (Figure 1f) was set as the irrigation source in all three valleys except for one-third of the Coachella Valley, which is irrigated using groundwater (CVWD, 2021). Given the lack of pumping locations data, the HRUs irrigated with groundwater were randomly selected. The initial maximum irrigation depths for each of the 15 agricultural land covers are shown in Table S1. Note that irrigation is applied directly to the first soil layer in SWAT. If the maximum irrigation depth for a given

HRU exceeds the available soil storage capacity, the remnant is returned to the original irrigation water source.

Daily records of precipitation and temperature from 160 gauges and 133 stations, respectively, were obtained from the NOAA Global Historical Climatology Network (Menne, Durre, Korzeniewski, et al., 2012; Menne, Durre, Vose, et al., 2012) and the California and Baja California Irrigation Management Information Systems (DWR-CIMIS, 2020; SIMAR-BC, 2020) and interpolated using the inverse distance weighting (IDW) method to estimate subbasin scale forcing for the 1980-2019 period. Relative humidity, solar radiation, and wind speed were estimated by the SWAT built-in weather generator using the 1979-2014 global weather dataset generated by the NCEP Climate Forecast System Reanalysis (Saha et al., 2014).

The Salton Sea was represented as a water HRU with a reservoir using a controlled release scheme, and the volume and surface area at the emergency spillway were set to the maximum lake water elevation (-67.1 m) reported in the most recent sediment survey data (Bureau of Reclamation, 1995). The volume at the principal spillway was assumed to be one-fourth of the emergency spillway and the average daily principal spillway release rate was set to 0 m^3 s^{-1}. The lake surface area was estimated through a rational regression model based on the elevation-area-capacity curves, and the lake evaporation coefficient and lakebed hydraulic conductivity were adjusted during calibration. Note that water HRUs areas were set to zero to avoid double counting of lake evaporation.

Model simulations were conducted at a daily time step from January 1, 1980, to December 31, 2019 (40 years), with the first five years as a warm-up period. Runoff calculation is based on the curve number approach and to mimic the SSTB complex water distribution system, point sources, water transfers, and consumptive water uses were implemented in the model. Inflows from the Colorado River at the All-American Canal below the Pilot Knob (USGS 09527500) and the Morelos Dam (USGS 09522030), as well as those from the Colorado River Aqueduct at the Whitewater River Groundwater Replenishment Facility, were set up as point sources in SWAT based on daily records and annual reports (USGS, 2016), respectively. Correlation analysis and visual hydrograph assessment showed that the Groundwater Replenishment Facility is the only major recharge facility in the north influences Whitewater River flows and the Salton Sea budget. In the south, the water transfers from the All-American Canal and Canal Alimentador Central to nearby canals were defined using constant flow ratios based on the agricultural land areas and the irrigation depths shown in Table S1. SWAT built-in management tool for consumptive use was implemented to replicate losses from the system for municipal supply in the subbasins along the main stem of the Whitewater River that passes through Palm Springs, Cathedral City, and Rancho Mirage. These losses were varied monthly and adjusted during calibration. Any remaining flows not used for irrigation from the lateral canals in the three valleys (Figure 1f) were considered as losses from the system. The Canal Alimentador Central's losses were equal to the expected

deliveries to the Tijuana Aqueduct (i.e., 4.0-5.3 m^3 s^{-1}).

2.3 Model calibration and evaluation

The model performance was evaluated against historical monthly potential evapotranspiration (ETo) (DWR-CIMIS, 2020; SIMAR-BC, 2020), streamflow, and lake water level at 17, 24, and one gauging stations, respectively. The records at each gauge were randomly split into 70% for calibration and 30% for evaluation to prevent overfitting. SWAT lake evaporation estimates were also compared against lake evaporation estimates from the aerodynamic method (McMahon et al., 2013) using the meteorological records of the three nearest weather stations to the lake (i.e., CIMIS 136, 141, and 181; Figure S1; Table S2) for the 1997-2019 period (DWR-CIMIS, 2020). Given the lack of field measurements, this approach improved the lake evaporation coefficient and lakebed hydraulic conductivity estimates and reduced uncertainty of the lake evaporation and seepage losses. The SPE (before known as SUFI-2) algorithm (Abbaspour, 2020; Abbaspour et al., 2007) of the SWAT-CUP Premium software v6.1.1 was used to identify the best fitting model at each monitoring station by maximizing the Kling-Gupta Efficiency coefficient (KGE) (Gupta et al., 2009). Additional objective functions such as the Nash-Sutcliffe Efficiency coefficient (NSE) (Nash & Sutcliffe, 1970) and the Percent Bias (PBIAS) (Gupta et al., 1999) were calculated for model performance evaluation. Annual actual evapotranspiration and crop yield were compared against available yield data for the Coachella and Imperial Valleys for some of the simulation years (Bureau of Reclamation, 2014; USDA-NASS, 2009).

2.4 Water balance assessment

Long-term water balance assessment helps to understand hydrological interactions in complex landscapes and reveals potential dependences of the lake dynamics to fluxes. The water balance of the SSTB is presented for the land-phase, stream, and the lake as simulated by SWAT (Figure 2).

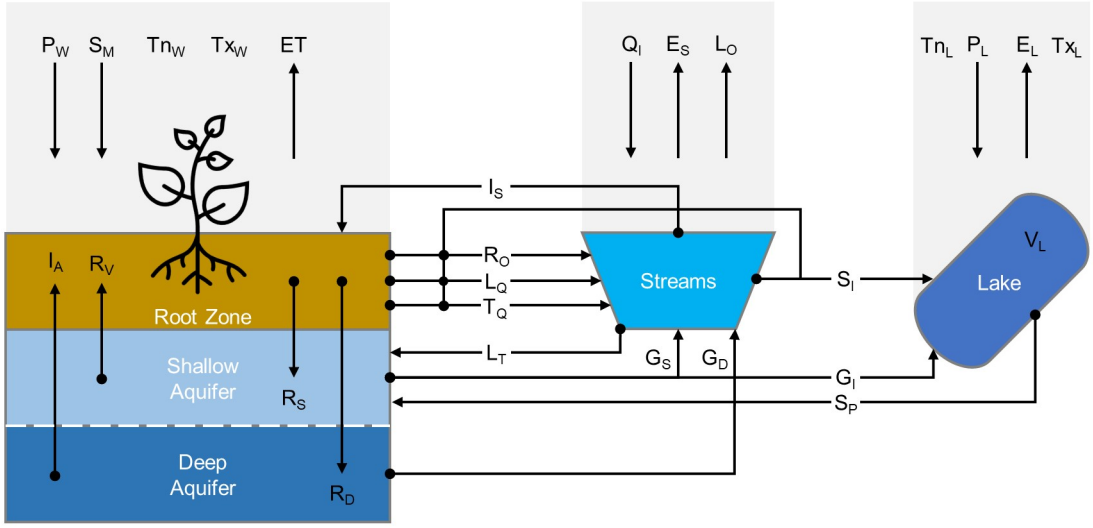

Figure 2. SWAT water balance for the SSTB considering lake-basin interactions.

According to SWAT conceptualization, the water balances of the basin and its root-zone, stream, and lake subsystems (Figure 2) are calculated as follow:

$$S_W = P_W + S_M + Q_I + I_A + G_D + P_L - ET - E_S - L_O - E_L \quad (1)$$

$$S_{\mathrm{RZ}} = P_W + S_M + I_S + I_A + R_V - ET - R_S - R_D - R_O - L_Q - T_Q \quad (2)$$

$$S_S = Q_I + R_O + L_Q + T_Q + G_S + G_D - E_S - L_O - I_S - L_T - S_I \quad (3)$$

$$S_L = P_L + S_I + G_I - E_L - S_P \quad (4)$$

where S_W, S_{RZ}, S_S, and S_L are the water storage change in the basin, root zone, stream, and lake systems, respectively. P_W and P_L are precipitation over the basin and lake, respectively. ET is basin evapotranspiration, and evaporation from stream (E_S), and lake (E_L) are calculated separately. S_M is snowmelt, Q_I is water imports from external sources, and L_O is other system losses (e.g., deliveries to external water bodies). I_S and I_A correspond to irrigation extracted from the stream and aquifer. R_V is the shallow aquifer contribution to the root zone by capillary rise, and R_S and R_D are the recharge to the shallow and deep aquifers, respectively. The stream system also receives contributions from the root zone and aquifer system though runoff (R_O), lateral flow (L_Q), tile flow (T_Q), and groundwater flow ($G_S + G_D$), and loses water via the streambed transmission losses (L_T). The lake water balance is altered by surface (S_I) and groundwater (G_I) inflows and outflows via seepage (S_P) and evaporation. Since lakes are simulated as reservoirs at specific point locations along the stream network, lake groundwater inflows are not explicitly simulated in SWAT, and were estimated as the difference between the tributary flows to the lake at gauging

locations (S_I) and the surface flows ($R_O + L_Q + T_Q$) from the non-water HRUs in subbasins with virtual streams.

2.5 Identifying the main drivers of lake level change

To assess the spatio-temporal relationships among the potential hydrologic drivers of the SSTB water balance changes, the seasonal-trend decomposition by locally estimated scatterplot smoothing (STL) (Cleveland et al., 1990) technique was employed. This technique decomposes a seasonal time series into three main additive components: trend, seasonal, and remainder (aka white noise), to identify the nonlinear relationships in long-term trends that cannot be identified using traditional linear regression (Shamsudduha et al., 2009). The advantage of using STL compared to other time series decomposition techniques is in its robustness to outliers and capability of handling any type of seasonality, and its change over time (Hyndman & Athanasopoulos, 2018). The monthly time series of basin and lake precipitation and temperature and each of the SWAT-generated time series for the lake water balance components, valley crop evapotranspiration and irrigation volume, and streamflow at monitoring and Salton Sea intake locations (Figure 1f) were decomposed using the R Forecast package (Hyndman & Khandakar, 2008; R Core Team, 2019) with the seasonal smoothing parameter determined by the graphical diagnostic method of Cleveland et al. (1990). Stationarity of the seasonally adjusted time series (i.e., where the seasonal component was removed) were examined by using the Augmented Dickey-Fuller (ADF) and the Kwiatkowski-Phillips-Schmidt-Shin (KPSS) (Dickey & Fuller, 1979; Kwiatkowski et al., 1992) statistics to identify variables with varying mean and variance under time shifts that may be associated with the lake water level decline. It is recommended to implement both stationary tests to ensure that the time series are truly stationary.

Given the complexity of quantifying the relative contribution of potential hydrologic change drivers affecting the lake-basin budget dynamics, we implemented two clustering techniques. The first clustering technique is based on dimensionality reduction, where multiple structural characteristics extracted from the time series are used to discern their similarity (X. Wang et al., 2006). Specifically, we calculated the strength of the trend and seasonality of the analyzed time series from the STL decomposition to determine variables with similar degree of trend and seasonality through the k-means clustering. These metrics were computed following Hyndman and Athanasopoulos (2018)'s definition:

$$F_T = \max\left(0, 1 - \frac{\mathrm{Var}(R_T)}{Var(T_T) + Var(R_T)}\right) \quad (5)$$

$$F_S = \max\left(0, 1 - \frac{\mathrm{Var}(R_T)}{\mathrm{Var}(S_T) + Var(R_T)}\right) \quad (6)$$

Where the strength of the trend (F_T) and seasonality (F_S) vary between zero and one with one representing strongly trended or seasonal data. T_T, S_T, and R_T correspond to the trend, seasonal, and residual components of the STL generated time series, respectively. The second clustering technique is hierarchical and uses a point-based distance metric to measure similarity among distinct time series. This technique generates a dendrogram to represent the nested grouping of patterns and similarity levels at which groupings change (X. Wang et al., 2006). Some of the most widely used distance metrics are variations of the Minkowski metric (including the widely used Euclidean distance) and correlation-based approaches. Although easy to implement, these distance metrics present some limitations for time series with out-of-phase similarities. We employed dynamic time warping (DTW) to overcome this issue. DTW algorithm calculates an optimal alignment between two given time series that are locally out of phase following a non-linear approach (Ratanamahatana & Keogh, 2005). The hierarchical clustering was applied to the normalized trends of the basin and lake water balance components.

3 Results and Discussion

3.1 Water balance partitioning of a highly managed endorheic basin

3.1.1 Model performance assessment

SWAT model performance was satisfactory in simulating temporal patterns of monthly ETo, streamflow, and lake storage across the SSTB. The KGE (0.85-0.97), NSE (0.73 0.95) and PBIAS (-10.6% 9.6%) in 16 of the 17 ETo monitoring stations (Figures 1f, 3a, and S1; Table S2) indicated a very good fit between the observed and simulated values in both calibration and evaluation periods. These satisfactory results were achieved by using the Hargreaves' formulation in SWAT instead of the Penman-Monteith's method that overestimates ETo in water-stressed regions when daily mean meteorological values are used (Hua et al., 2020; Neitsch et al., 2011). The only exception is at the station Nuevo Leon (SIMAR 004; Figure S1; Table S2) where KGE (0.66-0.69) and NSE (0.61 0.64) values were lower and PBIAS (-19.0% -17.2%) were higher than other monitoring stations. The disagreement between the estimated and simulated ETo was most likely due to measurement errors.

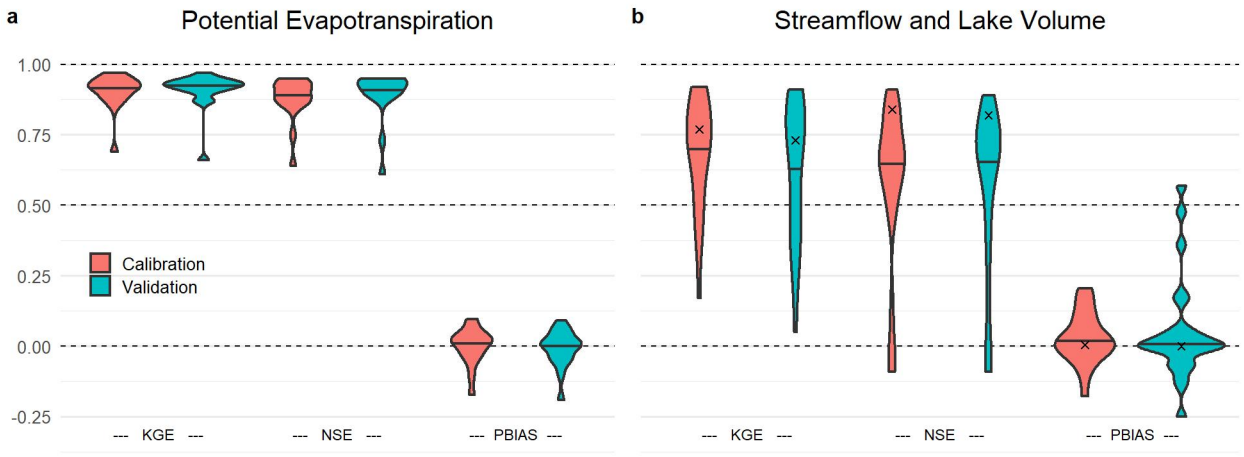

Figure 3. Violin plots of model performance metrics for (a) potential evapotranspiration and (b) streamflow and lake volume. The horizontal solid black lines depict the median of each distribution, and the cross markers represent the metric values for the lake volume. The PBIAS is presented as a ratio for visualization purposes.

Streamflow calibration was more challenging as streamflow is influenced by natural and human-induced hydrological processes, and observations about applied irrigation rates, water distribution system and transfers, and cropping systems are limited. The parameter range and calibrated parameters values are shown in Table S0. According to the ASABE guidelines for calibrating hydrologic and water quality models (ASABE, 2017), SWAT performance for simulating streamflow was satisfactory (NSE 0.5 and PBIAS 25%) across 75% and 64% of the gauges during calibration and evaluation, respectively (Figures 3b and S1; Table S3). Although the NSE and PBIAS values at some gauges were outside of the acceptable ranges, PBIAS was only significantly large at three gauges (i.e., USGS 10259100, 10259200, 10259300; Figure S1; Table S3) during the evaluation period. The KGE values for these gauges were above the mean flow benchmark (i.e., KGE = -0.41; Figure S1; Table S3) (Knoben et al., 2019), indicating that simulated streamflow is more accurate than the long-term mean. Overall, long-term water balance across the basin is well captured by the model, with the exception of the gauges near the urban areas along the Whitewater River (upstream of the Coachella Valley), where flows were fully withdrawn for municipal use.

The calibration and validation of the Salton Sea water budget showed good agreement between the estimated and simulated evaporation (KGE 0.77; NSE 0.81; PBIAS 1.0%) and lake volume (KGE 0.73; NSE 0.82; PBIAS 0.5%; Figure 3b; Table S3, gauge 25). While accuracy of these variables is influenced by the estimated lake evaporation coefficient (0.568) and lakebed hydraulic conductivity (0.077 mm hr^{-1}), no estimate of the lakebed hydraulic conductivity is

available. Several studies (Allen et al., 1966; ch2m, 2018; Tompson et al., 2008) have considered constant annual groundwater inflows and outflows in the Salton Sea water balance using rough estimates from well-yield-testing and auger-hole data. Our study provides a starting point to understand the lake-groundwater interactions in the Salton Sea and illustrates SWAT appropriateness for modeling complex hydrologic processes of a highly managed basin such as the SSTB. Future modeling work should focus on explicit coupling of surface water and groundwater processes using SWAT-MODFLOW (Bailey et al., 2016; Guzman et al., 2015).

3.1.2 Basin and lake water budgets

Figure 4 illustrates the annual water budgets for the SSTB, root-zone, streams, and the lake over the 1985-2019 period. The basin predominantly relies on the Colorado River water imports (Q_I; ~64%) and precipitation (P_W) constitutes ~34% of the input. Precipitation is highly variable over time (Figure4a), and its variability may explain streamflow anomalies across the SSTB, given the delicate balance between inflows and outflows. Almost 83% of the basin inflows are lost to evapotranspiration (ET) and lake evaporation (E_L) due to the desert climate and agricultural production in the valleys (Figure4a). Root-zone water balance partitioning indicates that approximately 41% of the inflows to the root zone is from irrigation ($I_S + I_A$) and almost 70% is lost to evapotranspiration (Figure4b). The remaining basin outflows (LO; ~17%), mainly representing transfers to external water bodies and other system losses (e.g., withdrawals for municipal use) are less variable over time (Figure4a).

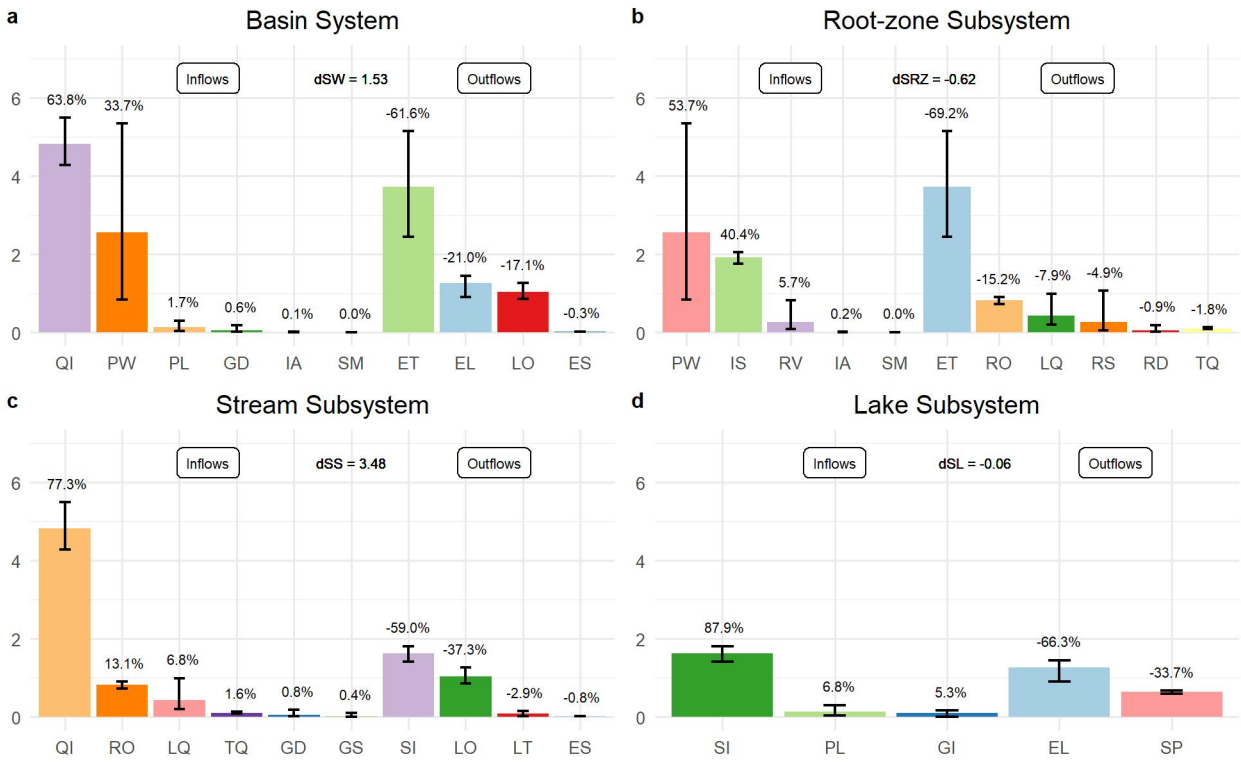

Figure 4. Annual water budget in km^3 for the (a) basin, (b) root-zone, (c) streams, and (d) lake based on equations 1-4 and Figure 2. The height of the color bars represents the long-term mean, while the black error bars indicate the minimum and maximum values over the 1985-2019 period. The percentages on the top of the error bars indicate the relative contribution of each component to the total inflows or outflows based on the long-term mean.

The main inflow to the stream subsystem is from the Colorado River (~77%), and 59% of its outflows discharge to the Salton Sea (Figure4c). For the lake, surface water inflows (S_I) represent the primary input (~88%), followed by significantly minor proportion of direct precipitation (P_L; ~7%) and groundwater inflow (G_I; ~5%) (Figure4d). Variability of precipitation and surface water inflows to the lake are similar over the simulation period. Given the endorheic nature of Salton Sea, the inputs are eventually lost to evaporation (E_L; ~66%) and seepage (S_P; ~34%) (Figure4d). The magnitudes of simulated lake evaporation and lake groundwater inflows agree with those estimated by Allen et al. (1966) and ch2m (2018) and Allen et al. (1966). Evaporation variability is larger than surface inflows and precipitation, and the higher variability of S_I, P_L, and E_L relative to other fluxes may explain lake water depletion. At the same time, the long-term change in lake storage (~-0.06 km^3 yr^{-1}) is approximately half of the groundwater inflows (~0.10 km^3 yr^{-1}) and half of the

direct precipitation (~0.13 km^3 yr^{-1}), comprising ~12% of the lake's inputs (Figure4d). Consequently, water balance components with insignificant magnitudes may play a key role in the lake water depletion. Time series analysis is required to identify nonstationary processes that are responsible for such depletion.

3.2 Major drivers of hydrologic variability and lake water depletion

3.2.1 Signs of depletion across the SSTB

Time series of the SSTB water balance components contain hydrologic signatures (i.e., characteristic signal information) that helps to discover similar patterns among various fluxes and storages, and hence, identify the major hydrologic drivers inducing Salton Sea depletion. Variability of the lake and basin water balance components based on the STL decomposition described a seasonal smoothing parameter between 49 and 61 years. The magnitude of the seasonal smoothing parameter indicates that the SSTB long-term seasonality has remained unchanged. Consequently, temporal fluctuations are more likely to be detected in the trend and remainder components of the analyzed time series. Time series decomposition results for the lake and relevant basin water balance components are shown in Figure 5.

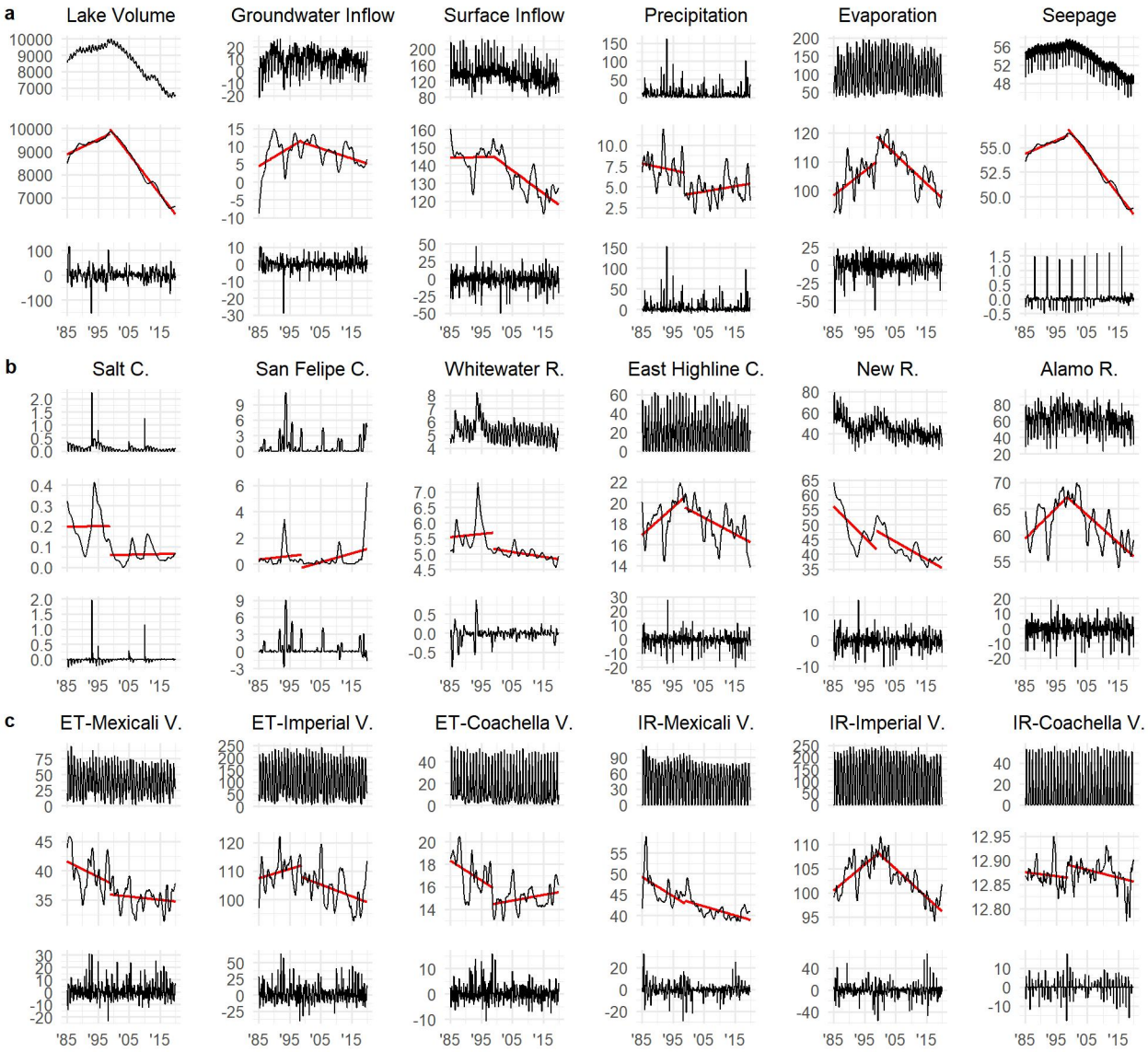

Figure 5. Monthly STL-decomposition results in Mm^3 for the processes relevant to influence the Salton Sea water depletion over the simulation period. (a) lake water balance components (Figures 2 and 4); (b) main lake tributaries and basin inflows; (c) valley evapotranspiration and irrigation. The top graphs correspond to the original time series, while the middle and bottom graphs correspond to the trend and remainder components, respectively. The red lines in the middle graphs are the linear regressions of the given variable before and after the inflection point in the lake volume trend was observed (November 1998).

The trend in monthly lake volume (V_L) explained most of its variability with a 3-km^3 range over the 1985-2019 period and a marked declining pattern (-0.17 km^3 yr^{-1}) after November 1998 (Figure 5a). This declining pattern coincides with the negotiation and implementation of the 1999 Colorado River Water Use 4.4 Plan, which required California to reduce its dependency on Colorado River surplus flows (~1 km^3 yr^{-1}) and return to its basic appropriation (~5.4 km^3 yr^{-1}) by 2016 (Water Education Foundation, 2022). At the same time, the 1998 conserved water transfer agreements (up to 247 Mm^3 yr^{-1} for up to 75 yrs.) between the Imperial Irrigation District and the San Diego County Water Agency became effective through the Quantification Settlement Agreement in October 2003 (Congressional Research Service, 2021; IID & SDCWA, 1998). All the Salton Sea water balance components had a similar declining trend to the lake volume (V_L) in late 1998 (Figure 5a) with the exception of precipitation (P_L) that was stationary over the simulation period using the KPPS and ADF tests. Hence, it is unlikely that precipitation is responsible for the Salton Sea depletion as it is not significantly changed over time.

The declining pattern in the lake evaporation (E_L) and seepage (S_P) trends (Figure 5a) mostly followed the lake volume. However, their declining trends are less likely to be the main cause of the lake depletion. In SWAT, seepage losses are simulated using a linear relationship between the lake surface area and the lakebed hydraulic conductivity, where the latter is constant over the simulation period. Therefore, the declining trend in seepage losses was not due to changes in the lake-groundwater interactions. Unlike the lake seepage, evaporation depends on the temporal variation of the lake surface area and the maximum and minimum temperatures used in the Hargreaves formulation to estimate ET_O. The maximum temperature across the basin was stationary over the simulation period by both the KPPS and ADF tests (i.e., non-varying mean and no unit root), while the minimum temperature has a non-stationary mean by the KPSS test. Although both the basin-wide and the near-lake minimum temperatures were non-stationary, only the near-lake minimum temperature depicted a decreasing trend (-0.068 °C yr^{-1}) after the lake water depletion began in late 1998. As a decrease in the minimum temperature would increase E_L per the Hargreaves formulation, this factor has an opposite effect to the decrease in lake surface area that lowers E_L. These feedbacks may explain slightly lower rate (-0.017 km^3 yr^{-1}) of lake outflows compared to inflows (-0.018 km^3 yr^{-1}) during late 1998 to 2019.

The Salton Sea depletion seems to be primarily caused by the decline in surface and groundwater inflows representing 93% of the lake inputs (Figure 4d). Specifically, surface and groundwater inflows, both with non-stationary means and trends declining at -0.0154 km^3 yr^{-2} and -0.0034 km^3 yr^{-2} (Figure 5a), respectively. The time series decomposition of the Salton Sea main tributaries in Figure 5b depict step changes in Salt and San Felipe Creeks, and Whitewater River flow trends, resulting in a lower mean flow after the lake volume inflection point in 1998. However, this drop in the mean flow coincides with the end of a wet period as shown by decline in precipitation after 1995 Figure 5a. On the

other hand, the trends in East Highline Canal, and New and Alamo Rivers flows declined as similar to V_L (Figures 5a-b). The declining trend in New River flow started from the beginning of the simulation period and differed from those of Alamo River and East Highline Canal (Figure 5b). This result suggest that the New River and Salton Sea depletion is likely caused by multiple factors and not solely by the 1999 Colorado River Water Use 4.4 Plan. The trends in crop ET and irrigation volume across the valleys (Figure 5c) resemble the patterns observed for the four major tributaries (i.e., Alamo, New, and Whitewater Rivers, and East Highline Canal; Figure 5b). Notice that crop ET and irrigation volume trends across the Mexicali Valley also depicted a declining trend from the beginning of the simulation period similar to the New River flow trend, implying that despite irrigation and drainage across the Imperial Valley, the New River flow may be predominantly driven by processes in the Mexican territory.

3.2.2 Hydrologic signatures across processes

The decomposed time series were further analyzed beyond their temporal variability through a characteristic-based k-means clustering using the strengths of their trend and seasonality (Eq. 5-6) to identify the major hydrologic drivers. Three optimal clusters were identified representing (Figure 6): (1) processes with weak trend and weak seasonality ($F_T < 0.5$; $F_S < 0.5$); (2) processes with weak trend but strong seasonality ($F_T < 0.5$; $F_S > 0.5$); and (3) processes with strong seasonality and strong trend ($F_T > 0.5$; $F_S > 0.5$). The Salt and San Felipe Creeks (i.e., Salton Sea minor tributaries) and all the headwater catchments' flows, except subbasin 69, were grouped with basin (P_W) and direct lake precipitation (P_L) in the first cluster (Figure 6). Like precipitation, flows at nine of the ten headwater catchments were stationary over the simulation period. The non-stationary flow corresponds to the Coyote Creek in subbasin 69 (USGS 10255810; Figure S1; Table S2), which is the only calibrated headwater catchment with direct human intervention (i.e., settlements and farming near and upstream of Borrego Springs). These results imply that precipitation is the main hydrologic driver in catchments where agriculture is not the primary land use and no significant shifts in the SSTB precipitation exist to explain alterations in the basin water budget or the Salton Sea depletion.

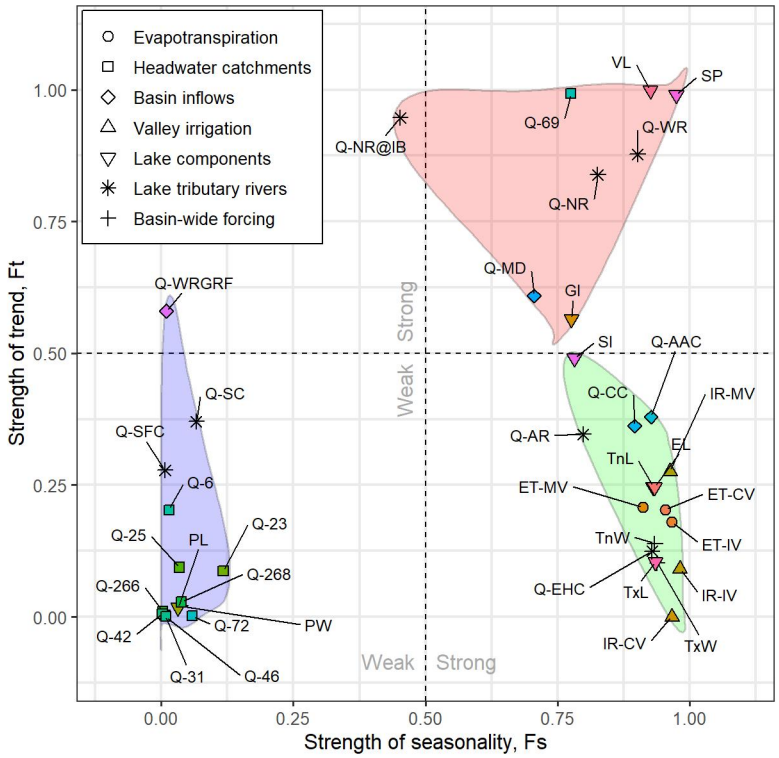

Figure 6. Characteristic-based clustering of SSTB main water balance components using the k-means clustering technique over the trend and seasonality strengths metrics.

The second cluster encompasses processes with a predominant seasonality that seem to be primarily driven by the SSTB and lower Colorado River Basin temperature. Applied irrigation volumes across the three valleys (Figure 5) driven by temperature through ET as well as lake evaporation are within this cluster. It is worth mentioning that S_I (i.e., lake surface inflows) was also part of this cluster, but only its major constituent, the Alamo River, had a similar strong seasonal pattern ($F_S > 0.75$) with a weak trend ($F_T < 0.5$). All-American and Coachella Canals flows also present the same behavior. Although the Colorado River management may be responsible for this outcome, the release scheduling of multiple dams and reservoirs follows the strong seasonal temperature variability from winter to summer. Consequently, the Alamo River flow variability seems to be inherited from the imported Colorado River water through the All-American Canal.

The third cluster characterized by processes with a strong trend and a strong seasonality ($F_T > 0.5$; $F_S > 0.5$; Figure 5), includes the lake volume (and seepage), groundwater inflows, Whitewater River flows, New River flows at the international border and near the Salton Sea, and the basin inflows at the More-

los Dam. From the lake surface inflows, New River is the tributary with the steepest declining pattern (-7.3 Mm^3 yr^{-2}; Figure 5b) after late 1998. This analysis confirms that the hydrologic signature of the imported Colorado River inflows through Mexican territory are sufficiently strong to be detected in the Salton Sea, and the declining New River flow is the major hydrologic driver of its depletion. However, Alamo River and East Highline Canal flows, declining at 6.4 and 2.7 Mm^3 yr^{-2} (Figure 4b), respectively, are also partially responsible for the Salton Sea depletion.

3.4 Interrelationships among lake depletion, irrigation, and imported Colorado River inflows

Salton Sea depletion was primarily caused by the decline in major tributaries inflows (i.e., New and Alamo Rivers, and East Highline Canal). Several studies and reports (Barnum et al., 2017; Cohen, 2014; Congressional Research Service, 2021; Doede & DeGuzman, 2020; Scott et al., 2014) have suggested that decline in the lake inflows is mostly due to four reasons: (1) lack of precipitation due to drought, (2) decreasing agricultural return flows caused by more efficient irrigation methods in the Imperial Valley, (3) decline in flows from Mexico, and (4) increasing water transfers to San Diego County. The latter can only affect the SSTB water balance through direct reductions in the Colorado River allocations, causes of which are out of the scope of this study as the Colorado River Aqueduct transfers water to San Diego County from the Lake Havasu in Arizona. Using time series decomposition and characteristic-based clustering, our results showed that precipitation has been stationary over time across the SSTB and flow deliveries from Mexico have been declining. Moreover, major Salton Sea tributary flows inherit their structural behavior (in terms of trend and seasonality strengths) from the imported Colorado River at All-American Canal and Morelos Dam. However, these findings do not necessarily imply that the declining trends in the New and Alamo Rivers, East Highline Canal, and the deliveries from Mexico relate to the Colorado River inflows or changes in irrigation practices across the Mexicali and Imperial Valleys.

In order to explore interrelationships between the main lake tributary inflows, the Colorado River inflows, and valley irrigation volumes, a hierarchical time-series clustering approach was implemented to partition trend and seasonal components of water balance variables into groups based on dynamic time warping similarity. Therefore, time series within a same cluster have similar patterns over time. Clustering results are shown in Figure 7, where the dendrogram nodes correspond to the analyzed variables. The distance between a given link and the node base represents the level of dissimilarity (0-500) among variables and subclusters. Based on the trend component, the analyzed variables were grouped into two major clusters representing processes directly affected by the Colorado River inflows in the American and Mexican territories (Figure 7a). In the first cluster, Alamo River and East Highline Canal flows were highly aligned with long-term trends in the All-American Canal inflow, and further related to the irrigation volumes at the Imperial and Coachella Valleys with a more signifi-

cant dissimilarity degree (>200; Figure 7a). These interrelationships prove that the Alamo River trend obeys Colorado River inflows variabilities rather than irrigation dynamics. In another words, the Colorado River inflows through the All-American Canal are the main driver of variability in the Alamo River and irrigation volume trends in the American territory.

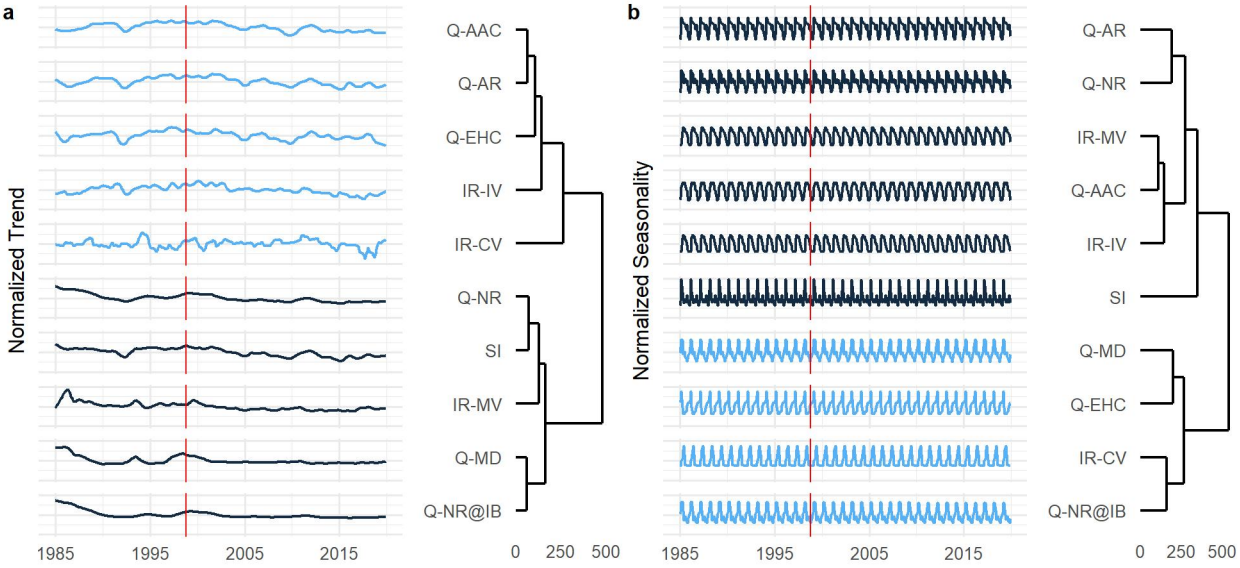

Figure 7. Hierarchical clustering for the normalized (a) trend and (b) seasonality of the lake main tributaries, Colorado River inflows, and valley irrigation volumes.

The second trends cluster shows that the New River flow at the international border well mimics the temporal variations of inflows at the Morelos Dam (Figure 7a). Similarly, the lake surface inflows (S_I) closely resembles the New River flow trend (Figure 7a), which was identified as the major driver of the Salton Sea depletion using the characteristic-based clustering (Figure 6). The irrigation volume trend of the Mexicali Valley was nested to the latter subcluster with more dissimilarity. Like the other two valleys, the decline in Colorado River inflow seems to induce these decreasing patterns. Unlike the Alamo River and the All-American Canal flow trends in the first cluster, the trend of the New River flow near the Salton Sea is not very similar to that of the Colorado River flows at the Morelos Dam (Figure 7a). Although both flow regimes possess similar structural behavior (i.e., strong trend and seasonality; Figure 6), the New River flow is altered through the American territory due to irrigation across the Imperial Valley derived from the All-American Canal's three major lateral canals (Figure 1).

Clustering of seasonality time series produced two main clusters. The largest cluster includes six variables grouped in three well defined subclusters (Figure

7b): (1) Salton Sea surface inflows, (2) New and Alamo Rivers flow, and (3) All-American Canal inflow nested with the irrigation volumes across the Mexicali and Imperial Valleys. The third subcluster configuration confirms that irrigation follows the Colorado River inflow dynamics, and although irrigation affects the major lake tributary flows, these flows are predominantly controlled by the Colorado River inflow dynamics. The remaining variables, i.e., the East Highland Canal and New River at the international border flows, Colorado River inflows at the Morelos Dam, and the Coachella Valley irrigation volume, were grouped in the second seasonality cluster with two subclusters (Figure 7b). Variables in both subclusters are characterized by peak values occurring in March-May. However, the hydrograph recession limb is steeper in the variables of the second cluster. It seems deliveries at the Morelos Dam are not sustained during the driest period of the year and affect the New River flow downstream of the international border. The East Highline Canal flow that reaches the Salton Sea follows surplus flows from the All-American Canal (i.e., not immediately used for irrigation) and losses from the drainage system, which decrease in the driest season. The atypical seasonality of the Coachella Valley irrigation may be due to its partial dependency on groundwater, which obeys different dynamics from those imposed by the Colorado River inflows through the Coachella Canal.

4 Conclusions

Quantifying the relative contribution of climate variability and anthropogenic stressors in water budget dynamics of endorheic lakes in highly managed agricultural landscapes is challenging as they are intertwined and highly variable in time and space. This study developed a diagnostic framework to detect spatio-temporal variability of water balance components and identify major hydrologic drivers of Salton Sea depletion by integrating SWAT with time-series data mining techniques. The implementation of characteristic-based and hierarchical clustering on decomposed time series can describe water-balance components' structural behavior and reveal seasonal and trend alterations traceable at the basin scale. The diagnostic framework was applied to the SSTB, where lake restoration is in the state and national interest given air quality issues and deterioration of internationally significant wildlife habitat.

Our results illustrate that decreases in the Colorado River allocation are causing the Salton Sea to shrink, not changes in the irrigation operation or local climate as commonly believed. Specifically, signs of depletion across the SSTB were identified in late 1998. While SSTB climate conditions have not significantly changed over time, the Salton Sea level have depleted by 32% due to the decline in major tributaries inflows (New River ~ -7.3 Mm^3 yr^{-2}; Alamo River ~ -6.4 Mm^3 yr^{-2}; East Highline Canal ~ -2.7 Mm^3 yr^{-2}). The structural (seasonality and trend strengths) analysis of the SSTB water balance components indicated that the hydrologic signature of the Colorado River inflows is strong through the Mexican and American territories and at the Salton Sea. Moreover, dynamic time warping established that the irrigation volume trends across the Mexicali, Imperial, and Coachella Valleys, are not the main drivers of depletion

in the lake tributaries. On the contrary, irrigation temporal variability is also explained by the Colorado River inflows dynamics. The negotiation and implementation of the 1998 conserved water transfer agreements and 1999 Colorado River Water Use 4.4 Plan concur with the SSTB water depletion. Although these agreements represent an annual decrease in Colorado River allocations of 1 km^3 for California and up to 247 Mm^3 for the Imperial Valley, it is not clear if their implementation is mainly causing the Salton Sea to shrink, or the decline of Colorado River inflows due to global warming, or both. A holistic approach that considers both basins is required to mitigate health and environmental impacts of Salton Sea depletion.

The modeling and multivariate attribution and detection framework developed in this study provides a robust basis for understanding spatio-temporal dynamics of lake-basin interactions and identifying main causes of lake depletion in a highly managed endorheic. Compared to trend detection or sensitivity analysis approached commonly used in attribution studies (Ayers et al., 2021; Ma et al., 2014; Villarini et al., 2020), the new framework takes advantage of multivariate signatures from decomposed time series and time warping methods to identify major drivers of hydrologic change. The detection and attribution framework can be used in other regions where detection and attribution of climate versus human-induced changes are of interest (Barnett et al., 2008).

Acknowledgments

This work is based upon work supported by the National Science Foundation (NSF) under Grant Addressing Decision Support for Water Stressed FEW Nevus Decisions Numbered 1739977. We would like to thank Dr. Ali Montazar for providing site specific information about cropping and irrigation patterns in the basin.

Open Research

The SWAT model code is open source and available on https://swat.tamu.edu/ and all the model forcing and parameterization datasets are publicly available. Daily simulation outputs will be placed on the UC Riverside 758 Dryad repository (link will be updated here once we have a manuscript ID to link the dataset to).

References

Abbaspour, K. C. (2020). *SWAT-CUP Premium User Manual*.

Abbaspour, K. C., Yang, J., Maximov, I., Siber, R., Bogner, K., Mieleitner, J., et al. (2007). Modelling hydrology and water quality in the pre-alpine/alpine Thur watershed using SWAT. *Journal of Hydrology*, *333*(2–4), 413–430. https://doi.org/10.1016/j.jhydrol.2006.09.014

Allen, G. H., Hughes, G. H., & Irelan, B. (1966). *Hydrologic Regime of Salton Sea, Caliornia*. Washington.

Arnold, J. G., Kiniry, J. R., Srinivasan, R., Williams, J. R., Haney, E. B., & Neitsch, S. L. (2012). *Input/Output Documentation Soil & Water Assessment Tool*.

ASABE. (2017). Guidelines for Calibrating, Validating, and Evaluating Hydrologic and Water Quality (H/WQ) Models, 15 pp.

Audubon California. (2021). Salton Sea. Retrieved June 16, 2021, from https://ca.audubon.org/salton-sea?page=1

Ayers, J. R., Villarini, G., Schilling, K., & Jones, C. (2021). On the statistical attribution of changes in monthly baseflow across the U.S. Midwest. *Journal of Hydrology*, *592*, 125551. https://doi.org/10.1016/j.jhydrol.2020.125551

Bailey, R. T., Wible, T. C., Arabi, M., Records, R. M., & Ditty, J. (2016). Assessing regional-scale spatio-temporal patterns of groundwater–surface water interactions using a coupled SWAT-MODFLOW model. *Hydrological Processes*, *30*(23), 4420–4433. https://doi.org/10.1002/hyp.10933

Barnett, T. P., Pierce, D. W., Hidalgo, H. G., Bonfils, C., Santer, B. D., Das, T., et al. (2008). Human-Induced Changes in the Hydrology of the Western United States. *Science*, *319*(5866), 1080–1083. https://doi.org/10.1126/science.1152538

Barnum, D. A., Bradley, T., Cohen, M., Wilcox, B., & Yanega, G. (2017). *State of the Salton Sea—A science and monitoring meeting of scientists for the Salton Sea*. Reston. https://doi.org/10.3133/ofr20171005

Bernal, J. M., Goff, A. L., Herrera Solis, J. A., & Bernal, F. A. (1999). *Flow of the Colorado River and other Western ounary Streams and Related Data*.

Bureau of Reclamation. (1995). 1995 Salton Sea sediment survey data. Retrieved November 7, 2020, from http://www.sci.sdsu.edu/salton/reservoir_sedimentTable1.html

Bureau of Reclamation. (2014). *2009-2014 Lower Colorado River Annual Summary of Evapotranspiration and Evaporation*. Boulder City. Retrieved from https://www.usbr.gov/lc/region/g4000/wtracct.html

ch2m. (2018). *Salton Sea Hydrology Development*. San Diego.

Cleveland, R. B., Cleveland, W. S., McRae, J. E., & Tarpenning, I. (1990). STL: A seasonal-trend decomposition procedure based on loess. *Journal of Official Statistics*, *6*(1), 3–73.

Cohen, M. J. (2014). *The Costs of Inaction at the Salton Sea*. Oakland. Retrieved from https://pacinst.org/publication/hazards-toll/

CONABIO. (2017). 2010 land cover of Mexico at 30 meters. Retrieved from file:///D:/Research/UCR/Salton_Sea/Data/Land_Cover/Mexico/Nation/nalcmsmx30gw.html

Congressional Research Service. (2021). *Salton Sea Restoration*. Retrieved from https://crsreports.congress.gov

CVWD. (2021). Agricultural Irrigation & Drainage. Retrieved September 20, 2021, from http://www.cvwd.org/166/Agricultural-Irrigation-Drainage

Dehghanipour, A. H., Schoups, G., Zahabiyoun, B., & Babazadeh, H. (2020). Meeting agricultural and environmental water demand in endorheic irrigated river basins: A simulation-optimization approach applied to the Urmia Lake basin in Iran. *Agricultural Water Management*, *241*, 106353. https://doi.org/10.1016/j.agwat.2020.106353

Dickey, D. A., & Fuller, W. A. (1979). Distribution of the Estimators for Autoregressive Time Series With a Unit Root. *Journal of the American Statistical Association*, *74*(366). https://doi.org/10.2307/2286348

Doede, A. L., & DeGuzman, P. B. (2020). The Disappearing Lake: A Historical Analysis of Drought and the Salton Sea in the Context of the GeoHealth Framework. *GeoHealth*, *4*(9). https://doi.org/10.1029/2020GH000271

Donnelly, J. P., King, S. L., Silverman, N. L., Collins, D. P., Carrera-Gonzalez, E. M., Lafón-Terrazas, A., & Moore, J. N. (2020). Climate and human water use diminish wetland networks supporting continental waterbird migration. *Global Change Biology*, *26*(4). https://doi.org/10.1111/gcb.15010

DWR-CIMIS. (2020). Weather station records. Retrieved September 24, 2020, from https://cimis.water.ca.gov/Default.aspx

Frie, A. L., Garrison, A. C., Schaefer, M. v., Bates, S. M., Botthoff, J., Maltz, M., et al. (2019). Dust Sources in the Salton Sea Basin: A Clear Case of an Anthropogenically Impacted Dust Budget. *Environmental Science & Technology*, *53*(16), 9378–9388. https://doi.org/10.1021/acs.est.9b02137

Gupta, H. V., Sorooshian, S., & Yapo, P. O. (1999). Status of automatic calibration for hydrologic models: Comparisson with multilevel expert calibration, *4*(2), 135–143.

Gupta, H. V., Kling, H., Yilmaz, K. K., & Martinez, G. F. (2009). Decomposition of the mean squared error and NSE performance criteria: Implications for improving hydrological modelling. *Journal of Hydrology*, *377*(1–2), 80–91. https://doi.org/10.1016/j.jhydrol.2009.08.003

Guzman, J. A., Moriasi, D. N., Gowda, P. H., Steiner, J. L., Starks, P. J., Arnold, J. G., & Srinivasan, R. (2015). A model integration framework for linking SWAT and MODFLOW. *Environmental Modelling and Software*, *73*, 103–116. https://doi.org/10.1016/j.envsoft.2015.08.011

Hely, A. G., Hughes, G. H., & Irelan, B. (1966). *Hydrologic Regimen of Salton Sea, California*. Washington D.C.

Hua, D., Hao, X., Zhang, Y., & Qin, J. (2020). Uncertainty assessment of potential evapotranspiration in arid areas, as estimated by the Penman-Monteith method. *Journal of Arid Land*, *12*(1), 166–180. https://doi.org/10.1007/s40333-020-0093-7

Hyndman, R., & Athanasopoulos, G. (2018). *Forecasting: principles and practice* (Second). Melbourne, Australia: OTexts. Retrieved from https://otexts.com/fpp2/

Hyndman, R., & Khandakar, Y. (2008). Automatic time series forecasting: The forecast package for R. *Journal of Statistical Software*, *27*(3). https://doi.org/10.18637/jss.v027.i03

IID. (2021). Water Transportation System. Retrieved September 8, 2021, from https://www.iid.com/water/water-transportation-system

ISRIC. (2020). SoilGrids. Retrieved September 15, 2020, from https://soilgrids.org

Jones, B. A., & Fleck, J. (2020). Shrinking lakes, air pollution, and human health: Evidence from California's Salton Sea. *Science of The Total Environment*, *712*, 136490. https://doi.org/10.1016/j.scitotenv.2019.136490

Knoben, W. J. M., Freer, J. E., & Woods, R. A. (2019). Technical note: Inherent benchmark or not? Comparing Nash–Sutcliffe and Kling–Gupta efficiency scores. *Hydrology and Earth System Sciences*, *23*(10). https://doi.org/10.5194/hess-23-4323-2019

Koluvek, P. K. (1964). *Irrigation and drainage practices in the Colorado River basin of California*. Fresno, CA.

Kottek, M., Grieser, J., Beck, C., Rudolf, B., & Rubel, F. (2006). World Map of the Köppen-Geiger climate classification updated. *Meteorologische Zeitschrift*, *15*(3). https://doi.org/10.1127/0941-2948/2006/0130

Kwiatkowski, D., Phillips, P. C. B., Schmidt, P., & Shin, Y. (1992). Testing the null hypothesis of stationarity against the alternative of a unit root. *Journal of Econometrics*, *54*(1–3), 159–178. https://doi.org/10.1016/0304-4076(92)90104-Y

Li, X., Cheng, G., Ge, Y., Li, H., Han, F., Hu, X., et al. (2018). Hydrological Cycle in the Heihe River Basin and Its Implication for Water Resource Management in Endorheic Basins. *Journal of Geophysical Research: Atmospheres*, *123*(2), 890–914. https://doi.org/10.1002/2017JD027889

Ma, X., Lu, X. X., van Noordwijk, M., Li, J. T., & Xu, J. C. (2014). Attribution of climate change, vegetation restoration, and engineering measures to the reduction of suspended sediment in the Kejie catchment, southwest China. *Hydrology and Earth System Sciences*, *18*(5), 1979–1994. https://doi.org/10.5194/hess-18-1979-2014

McMahon, T. A., Peel, M. C., Lowe, L., Srikanthan, R., & McVicar, T. R. (2013). Estimating actual, potential, reference crop and pan evaporation using standard meteorological data: a pragmatic synthesis. *Hydrology and Earth System Sciences*, *17*(4), 1331–1363. https://doi.org/10.5194/hess-17-1331-2013

Menne, M. J., Durre, I., Vose, R. S., Gleason, B. E., & Houston, T. G. (2012). An Overview of the Global Historical Climatology Network-Daily

Database. *Journal of Atmospheric and Oceanic Technology*, *29*(7), 897–910. https://doi.org/10.1175/JTECH-D-11-00103.1

Menne, M. J., Durre, I., Korzeniewski, B., McNeal, S., Thomas, K., Yin, X., et al. (2012). Global Historical Climatology Network - Daily (GHCN-Daily). https://doi.org/10.7289/V5D21VHZ

Meyer, J. L., & van Schilfgaarde, J. (1984). Case history: Salton Basin. *California Agriculture*, *38*(10).

Mohammed, I. N., & Tarboton, D. G. (2012). An examination of the sensitivity of the Great Salt Lake to changes in inputs. *Water Resources Research*, *48*(11). https://doi.org/10.1029/2012WR011908

Montazar, A. (2021). Personal communication.

Nash, J. E., & Sutcliffe, J. V. (1970). River flow forecasting through conceptual models part I - A discussion of principles. *Journal of Hydrology*, *10*(3), 282–290. https://doi.org/10.1016/0022-1694(70)90255-6

Neitsch, S. L., Arnold, J. G., Kiniry, J. R., & Williams, J. R. (2011). *Soil and Water Assessment Tool Theoretical Documentation*. College Station.

NRCS. (2016). U.S. General Soil Map (STATSGO2). Retrieved September 9, 2020, from https://websoilsurvey.sc.egov.usda.gov/App/WebSoilSurvey.aspx

Oren, A. (2013). Life at High Salt Concentrations. In E. Rosenberg, E. F. DeLong, S. Lory, E. Stackebrandt, & F. Thompson (Eds.), *The Prokaryotes* (4th ed.). Springer. https://doi.org/10.1007/978-3-642-30123-0

Pillsbury, A. F. (1957). Drainage in Irrigated Deserts. *California Agriculture*, 35–36.

Poggio, L., de Sousa, L. M., Batjes, N. H., Heuvelink, G. B. M., Kempen, B., Ribeiro, E., & Rossiter, D. (2021). SoilGrids 2.0: producing soil information for the globe with quantified spatial uncertainty. *SOIL*, *7*(1), 217–240. https://doi.org/10.5194/soil-7-217-2021

R Core Team. (2019). R: A language and environment for statistical computing. Vienna: R Foundation for Statistical Computing, Vienna. Retrieved from https://www.r-project.org/

Ratanamahatana, C. A., & Keogh, E. (2005). Three Myths about Dynamic Time Warping Data Mining. In *Proceedings of the 2005 SIAM International Conference on Data Mining*. Philadelphia, PA: Society for Industrial and Applied Mathematics. https://doi.org/10.1137/1.9781611972757.50

Saccò, M., White, N. E., Harrod, C., Salazar, G., Aguilar, P., Cubillos, C. F., et al. (2021). Salt to conserve: a review on the ecology and preservation of hypersaline ecosystems. *Biological Reviews*, brv.12780. https://doi.org/10.1111/brv.12780

Saha, S., Moorthi, S., Wu, X., Wang, J., Nadiga, S., Tripp, P., et al. (2014). The NCEP Climate Forecast System Version 2. *Journal of Climate*, *27*(6), 2185–2208. https://doi.org/10.1175/JCLI-D-12-00823.1

Schulz, S., Darehshouri, S., Hassanzadeh, E., Tajrishy, M., & Schüth, C. (2020). Climate change or irrigated agriculture – what drives the water level decline of Lake Urmia. *Scientific Reports*, *10*(1), 236. https://doi.org/10.1038/s41598-019-57150-y

Scott, C. A., Vicuña, S., Blanco-Gutiérrez, I., Meza, F., & Varela-Ortega, C. (2014). Irrigation efficiency and water-policy implications for river basin resilience. *Hydrology and Earth System Sciences*, *18*(4), 1339–1348. https://doi.org/10.5194/hess-18-1339-2014

Shamsudduha, M., Chandler, R. E., Taylor, R. G., & Ahmed, K. M. (2009). Recent trends in groundwater levels in a highly seasonal hydrological system: the Ganges-Brahmaputra-Meghna Delta. *Hydrology and Earth System Sciences*, *13*(12). https://doi.org/10.5194/hess-13-2373-2009

Sheng, Y. (2020). Endorheic Lake Dynamics: Remote Sensing. In *Fresh Water and Watersheds* (First, pp. 33–43).

SIGA-BC. (2016). Area sown by crop group across the Mexicali Valley. Retrieved September 17, 2020, from http://www.sigabc.gob.mx/sigabc/

SIMAR-BC. (2020). Weather station records. Retrieved September 24, 2020, from http://www.simarbc.gob.mx/

State of California Salton Sea Management Program. (2021). Improving conditions at California's Salton Sea. Retrieved June 16, 2021, from https://saltonsea.ca.gov/

Tian, Y., Zheng, Y., Zheng, C., Xiao, H., Fan, W., Zou, S., et al. (2015). Exploring scale-dependent ecohydrological responses in a large endorheic river basin through integrated surface water-groundwater modeling. *Water Resources Research*, *51*(6), 4065–4085. https://doi.org/10.1002/2015WR016881

Tompson, A., Demir, Z., Moran, J., Mason, D., Wagomer, J., Kollet, S., et al. (2008). *Groundwater Availability Within the Salton Sea Basin*. Livermore.

USDA-NASS. (2009). CropScape - Cropland Data Layer. Retrieved September 19, 2020, from https://nassgeodata.gmu.edu/CropScape/

USGS. (2016). National Water Information System data available on the World Wide Web (USGS Water Data for the Nation). Retrieved October 4, 2020, from http://waterdata.usgs.gov/nwis/

USGS. (2019). 1 arc-second resolution Digital Elevation Model (publishe 2019-2020). Retrieved August 31, 2020, from https://apps.nationalmap.gov/downloader/#/

USGS. (2020). National Hydrography Dataset for Hyologic Unit (HU) 8. Retrieved September 19, 2020, from https://apps.nationalmap.gov/downloader/#/

Villarini, G., Zhang, W., Quintero, F., Krajewski, W. F., & Vecchi, G. A. (2020). Attribution of the impacts of the 2008 flooding in Cedar Rapids (Iowa) to anthropogenic forcing. *Environmental Research Letters*, *15*(11), 114057. https://doi.org/10.1088/1748-9326/abc5e5

Wang, J., Song, C., Reager, J. T., Yao, F., Famiglietti, J. S., Sheng, Y., et al. (2018a). Recent global decline in endorheic basin water storages. *Nature Geoscience*, *11*(12), 926–932. https://doi.org/10.1038/s41561-018-0265-7

Wang, J., Song, C., Reager, J. T., Yao, F., Famiglietti, J. S., Sheng, Y., et al. (2018b). Recent global decline in endorheic basin water storages. *Nature Geoscience*, *11*(12), 926–932. https://doi.org/10.1038/s41561-018-0265-7

Wang, X., Smith, K., & Hyndman, R. (2006). Characteristic-Based Clustering for Time Series Data. *Data Mining and Knowledge Discovery*, *13*(3), 335–364. https://doi.org/10.1007/s10618-005-0039-x

Water Education Foundation. (2022). Colorado River Water Use 4.4. Retrieved October 21, 2021, from https://www.watereducation.org/aquapedia/colorado-river-water-use-44-plan

Williams, W. D. (2002). Environmental threats to salt lakes and the likely status of inland saline ecosystems in 2025. *Environmental Conservation*, *29*(2), 154–167. https://doi.org/10.1017/S0376892902000103

Wright, M. N., & Ziegler, A. (2017). Ranger: A Fast Implementation of Random Forests for High Dimensional Data in C++ and R. *Journal of Statistical Software*, *77*(1). https://doi.org/10.18637/jss.v077.i01

Yao, F., Wang, J., Yang, K., Wang, C., Walter, B. A., & Crétaux, J.-F. (2018). Lake storage variation on the endorheic Tibetan Plateau and its attribution to climate change since the new millennium. *Environmental Research Letters*, *13*(6), 064011. https://doi.org/10.1088/1748-9326/aab5d3

Yapiyev, V., Sagintayev, Z., Inglezakis, V., Samarkhanov, K., & Verhoef, A. (2017). Essentials of Endorheic Basins and Lakes: A Review in the Context of Current and Future Water Resource Management and Mitigation Activities in Central Asia. *Water*, *9*(10), 798. https://doi.org/10.3390/w9100798

Yapiyev, V., Samarkhanov, K., Tulegenova, N., Jumassultanova, S., Verhoef, A., Saidaliyeva, Z., et al. (2019). Estimation of water storage changes in small endorheic lakes in Northern Kazakhstan. *Journal of Arid Environments*, *160*, 42–55. https://doi.org/10.1016/j.jaridenv.2018.09.008

Zadereev, E., Lipka, O., Karimov, B., Krylenko, M., Elias, V., Pinto, I. S., et al. (2020). Overview of past, current, and future ecosystem and biodiversity trends of inland saline lakes of Europe and Central Asia. *Inland Waters*, *10*(4), 438–452. https://doi.org/10.1080/20442041.2020.1772034

Zhou, J., Wang, L., Zhang, Y., Guo, Y., Li, X., & Liu, W. (2015). Exploring the water storage changes in the largest lake (Selin Co) over the Tibetan Plateau

during 2003–2012 from a basin-wide hydrological modeling. *Water Resources Research*, *51*(10), 8060–8086. https://doi.org/10.1002/2014WR015846